



NLR-TP-2005-366

Winglets on large civil aircraft: impact on wing deformation

B.B. Prananta, A. Namer*, J.E.J. Maseland, J. van Muijden and
S.P. Spekrijse

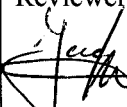
* Airbus France

This report has been based on a paper presented at the International Forum on Aeroelasticity and Structural Dynamics IFASD 2005, Munich, Germany, June 28th- July 1st, 2005. This report is deliverable D2.2.4-11 of the AWIATOR project.

This report may be cited on condition that full credit is given to NLR and the authors.

Customer: National Aerospace Laboratory NLR
Working Plan number: AV.1.E
Owner: National Aerospace Laboratory NLR
Division: Aerospace Vehicles
Distribution: Unlimited
Classification title: Unclassified
June 2005

Approved by:

Author	Reviewer	Managing department
 12/07/05	 12-07-2005	 12/7/2005



Summary

The impact of winglets of different size on the actual flight shape of the wing of a large civil aircraft is investigated. Three configurations are addressed: the standard winglet, a large winglet, and the clean wing for reference. The purpose of the investigation is to gain understanding of the aeroelastic behaviour of an integrated flexible wing and winglet combination. Verification of methods for the prediction of the actual flight shape of the wing at various cruise conditions is performed by comparison with optical measurements of the in-flight deformations. It is concluded that current aeroelastic prediction methods, based on Navier-Stokes flow modelling, provide a suitable analysis tool for baseline and trade-off studies of flexible aircraft.



Contents

1	Introduction	7
2	Flight Measurement	7
2.1	Some definitions	8
2.2	Aircraft instrumentation	8
2.3	Flight tests	9
3	Analysis Method	10
3.1	Aerodynamic model and mesh generation	12
3.2	Structural model	13
3.3	Coupling aerodynamic and structural models	14
3.4	Grid deformation	15
4	Results	16
4.1	Preliminary static aeroelastic simulations	16
4.2	Comparison with flight test	17
4.3	Comparisons between configurations	20
5	Concluding Remarks	22
6	References	23



List of symbols, subscripts and abbreviations

M	Mach number
C_L	Lift coefficient
[a]	Flexibility matrix
\bar{x}	Vector representing the state of the geometry
\bar{F}	Force vector
$d\bar{x}$	Vector of deformation
L_{ref}	Reference length

Abbreviations

AOA	Angle-of-attack
RANS	Reynolds-Averaged Navier-Stokes
LES	Large Eddy Simulation
FEM	Finite Element Method

Subscripts

deformed	Deformed state
aerodynamic	Contribution due to aerodynamic force
inertia	Contribution due to inertial force
thrust	Contribution due to thrust force
ground	A hypothetical deformation state on the ground due to inertial and thrust forces but with landing gear retracted
flight	The state of geometry during flight
jig	Jig shape, manufacturing shape
augmentation	Pre-deformed shape to assist deformation computation



This page is intentionally left blank.



1 Introduction

Large modern civil aircraft pose a tremendous challenge in wing design. The inherent flexibility of the configuration needs to be considered in order to identify whether the set of requirements for the aircraft is met. Current analysis tools, based on CFD-methods, include the possibility to calculate the actual deformations of the configuration at cruise and at off-design condition. The present paper addresses the impact of winglets of different size on wing deformation and flow characteristics.

In current aircraft design, the wings achieve their most efficient shape for a particular cruise condition in terms of speed and weight. The wing flight shape is usually optimised for a specific cruise Mach number and lift coefficient. The jig-shape of the wing is retrofitted from the flight shape by applying appropriate static aeroelastic deformations, and is manufactured accordingly. In view of this methodology, the optimal application of winglets on aircraft wings requires its inclusion at a sufficiently early stage in the design process, i.e. at least before the jig-shape is defined, but preferably even during the design of the flight shape. Since winglets, or winglet enlargements, are sometimes also used in an attempt to improve the operational behaviour of existing wings, the actual flight shape of the wing needs to be verified. It is mandatory to assess the envelope of beneficial impact of the winglet.

In this paper, the methodology to analyse the deformations of the wing with different types of winglets is described, and results from applications are discussed. Part of the work has been performed within the European project AWIATOR (Aircraft Wing with Advanced Technology Operation).

2 Flight measurements

During operational use, an aircraft is subjected to a large number of flight conditions. Since the wing is flexible, the varying aerodynamic and inertia loads induce variations in wing twist and wing bending. To enable realistic aircraft performance assessment, it is of utmost importance to be able to predict the wing shape accurately during the flight. Consequently, a good knowledge of the effects of loads on the wing shape is essential. Therefore, in the AWIATOR project, flight measurements have been carried out to investigate the wing deformation due to several types of winglets and to validate the computational methods.



2.1 Some definitions

Depending on the loads applied on the wing, three main wing shapes are to be distinguished: the jig shape, the ground shape and the flight shape.

The jig shape is the shape of the wing that is not affected by fuel, gravity and aerodynamic loads. For a given aircraft this shape is unique.

The ground shape is the shape of the wing that is affected by gravity and the fuel distribution. No aerodynamic load is taken into account. Contrary to the jig shape, the ground shape is not unique. It varies with the fuel distribution and the type of manoeuvre. Moreover, for one fuel distribution, two different ground shapes exist: the ground shape where the aircraft rests on its landing gear and the ground shape without landing gear. The latter shape is only theoretical but is widely used for flexible CFD calculations.

The flight shape is the wing shape when all the loads are taken into account. The gravity, the fuel distribution and the aerodynamic loads deform the jig shape into the flight shape. This shape changes during the flight because of the variation of fuel quantity and flight conditions. Concerning the bending and twist measurements of the wing, the results are presented as the deformation in the z-direction and rotation in the y-direction at a location one-third chord from the leading edge. Since the wing of the test aircraft has a significant sweep angle and the structural layout of the ribs is perpendicular to the wing sweep there is a coupling between the bending and twist of the wing. An increase of the wing bending generates a nose-down twist.

2.2 Aircraft instrumentation

Two types of instrumentation have been incorporated during the flight measurements, namely the optical instrumentation to measure the deformation and instrumentation for pressure measurements. In the present paper, only the wing deformation will be discussed. The optical instrumentation consists of several targets located on the right wing, see Figure 1, and high-resolution cameras installed in the cabin. Since the targets slightly protrude into the airflow it may disturb the flow above the right wing, although this effect is expected to be insignificant. The wing deformation is obtained through a photogrammetric technique. The spanwise positions of the targets are located at 32.5%, 50%, 67.5%, 81%, 93% and 99% of the wing semi-span, with additional targets on the large winglet when used. The accuracy of data provided is expected to be $\pm 0.1^\circ$ at the wing tip.



Figure 1 Overview of the targets on the starboard wing for deformation measurement

2.3 Flight tests

In order to cover a wide range of wing deformations that can occur during normal operation, various flight points have been flown out. The range of Mach number at which the flight test has been carried out is between $M=0.80$ and $M=0.84$, but most of the measurements are accomplished at Mach 0.82 for three different aircraft weights. When flying at constant Mach number, the main parameters varying during the flight would be the aircraft weight (therefore the lift C_L) and the flight altitude. Due to ordinary air traffic control implications during cruise, however, the flight takes place at constant altitude within a C_L range at which the wing has been optimised, see Figure 2. Therefore, during a flight the wing shape will then be modified by a change of altitude and of lift coefficient C_L . The wing can also undergo deformations stemming from a change of Mach number.

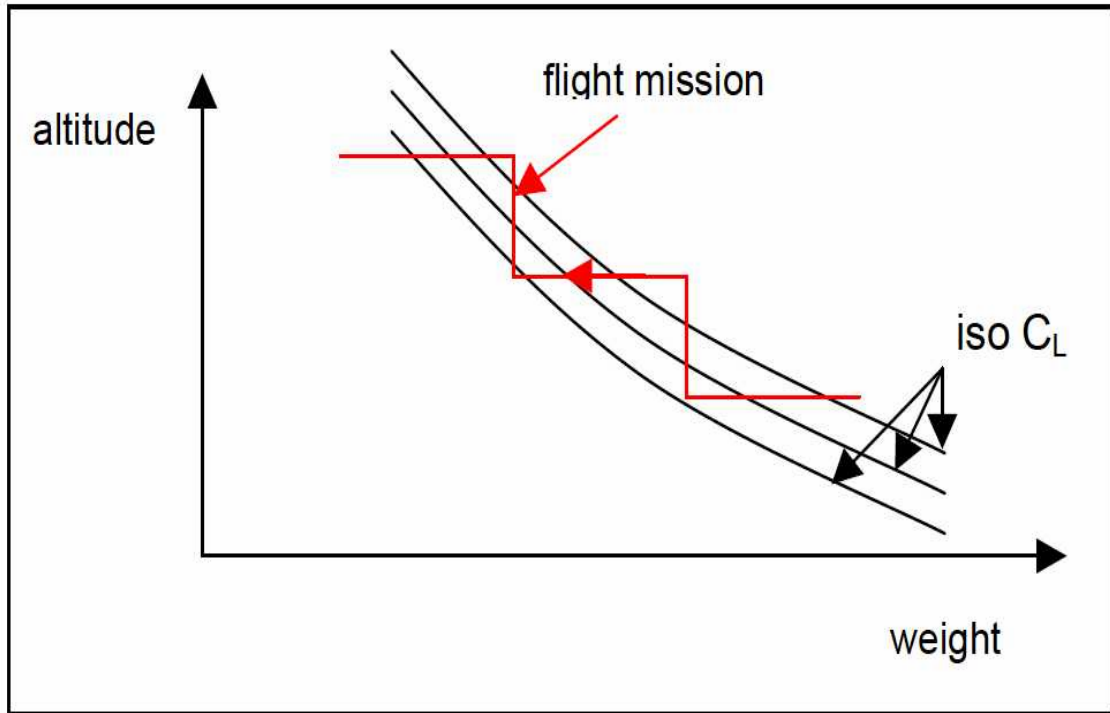


Figure 2 Schematic diagram of a typical flight mission during deformation measurement

3 Analysis Method

The results of numerical simulations presented in the present work have been obtained using the NLR ENFLOW system. The ENFLOW system is the NLR in-house developed multi-purpose CFD-system suitable for solving either the Euler or Navier-Stokes flow equations on multi-block structured meshes from incompressible flow up to supersonic flow. State-of-the-art two-equation models are available for efficient and accurate representation of the turbulence in a Reynolds-averaged fashion. More advanced flow modelling includes the hybrid RANS/LES approach to turbulence. The ENFLOW system has been extensively applied for a wide range of applications ranging from aircraft aerodynamics, acoustics, internal cabin flow analyses up to aeroelasticity of aircraft.

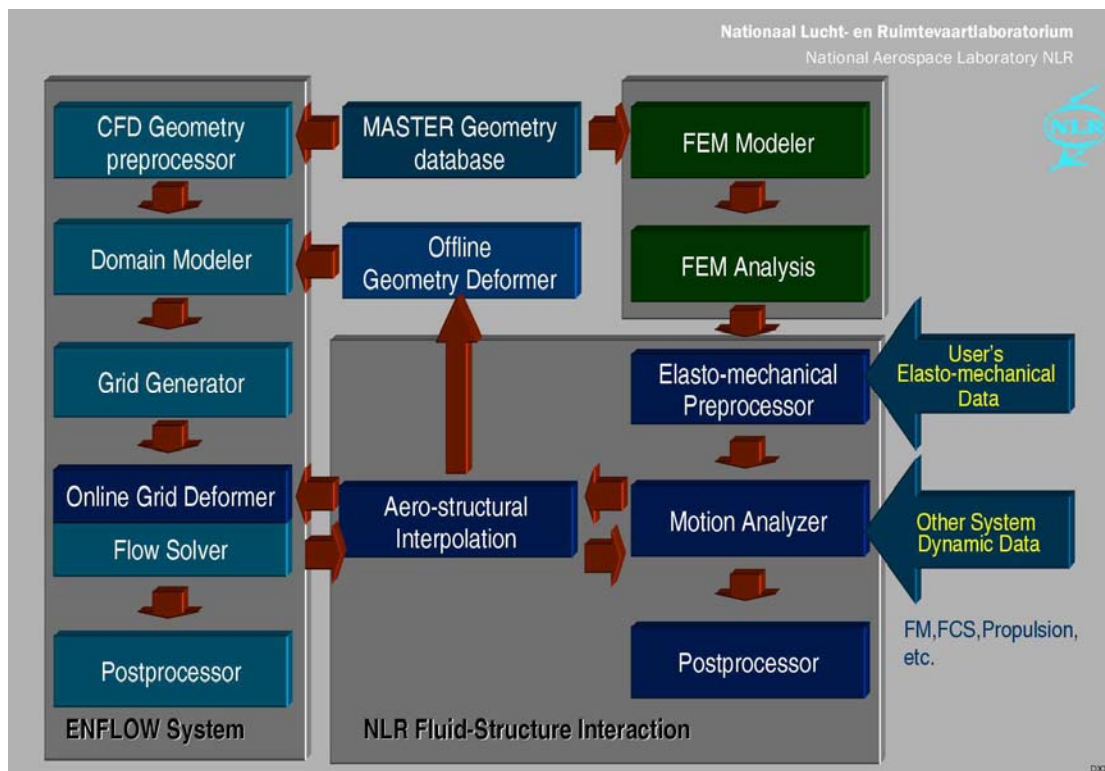


Figure 3 Schematic diagram of ENFLOW system with aeroelastic capability

In coping with various types of research, the flow solver of the ENFLOW system, ENSOLV, has been coupled with various models, including the equations of motion of flexible aircraft. The later has been developed to enable both static and dynamic aeroelastic analyses of aircraft. The methods and applications of ENSOLV have been reported previously for static aeroelastic applications [1] and dynamic aeroelastic applications [2]. The static aeroelastic capability of the ENFLOW system includes:

Simulation of a restrained or free flight condition, the latter is typified by a balance between the inertial and aerodynamic forces and moments.

Simulation for a given flow condition, e.g. angle of attack and side slip angle, or inclusion of trim analyses to reach a given flight attitude, e.g. load factors. In the first situation the deformed aircraft state is part of the solution while in the second situation the trim module seeks for the best combination of angle of attack and control surface deflections, to satisfy the required load factors.

Various post-processing options of the loads data are available, e.g. aerodynamic and inertial loads at arbitrary cuts of the structure or mapped to a set of nodes, e.g. the nodes of the finite element model for the stress analysis.

The elements of the method are sketched in Figure 3, namely the flow solver, the grid deformer, the structural solver and the fluid-structure coupling module. The fluid-structure coupling



module takes care of the interaction of the structural solver and the flow solver in time and space. The communication between the flow solver and structural solver is carried out through the fluid-structure interface that consists of the aerodynamic surface grid, the structural surface grid and the interpolation matrix connecting these surface grids. The interpolation matrix handles the mapping of aerodynamic loads from the aerodynamic grid to the structural grid and vice versa for the mapping of the structural deformation. Once the aerodynamic surface grid gets the deformation from the structural model, the grid deformer spreads the deformation into the spatial grid. The synchronisation between the aerodynamic and structural states is carried out in an iterative manner. Usually the states are updated after a number of aerodynamic iterations. For steady problems the synchronised condition is reached at the end of the simulation. For unsteady problems it is reached at every time step which means that the method is as accurate as a fully coupled method.

For the analysis of the problem at hand, i.e. a wing with large winglet, some special provisions of the method have been included. These provisions were necessary to accommodate the available structural data efficiently and to handle the reference wing shape. In the following sections these special provisions are detailed.

3.1 Aerodynamic model and mesh generation

For the purpose of accurate deformation predictions, the selected aerodynamic model in the present study is the full Reynolds-averaged Navier-Stokes flow model. The usage of a state-of-the-art Navier-Stokes flow model is at present performed on a routine basis, and the resulting aerodynamic loads are of high quality, also in cases of shock-wave boundary-layer interaction and flows including areas with separation. Turbulence is taken into account by using a two-equation $k-\omega$ model. The computations are performed assuming a fully turbulent boundary layer, which is in general consistent with flight test conditions. Turn-around times of the flow solver including deformations of the mesh are comparable to Navier-Stokes computations on a rigid configuration.

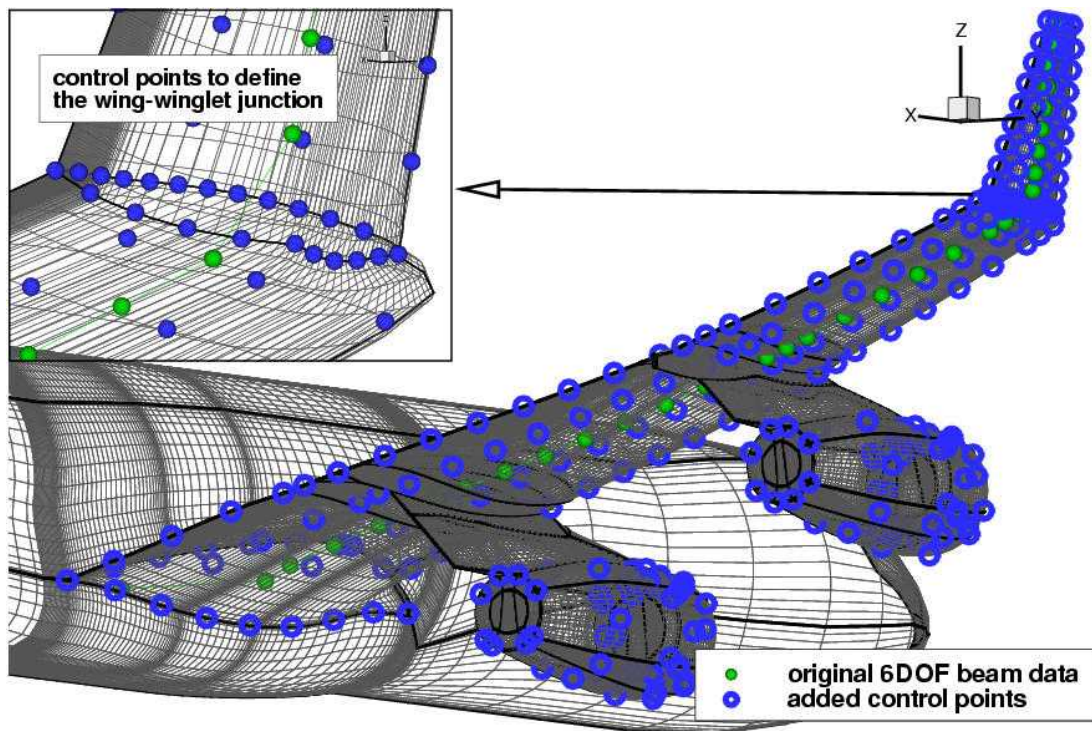


Figure 4 The aerodynamic surface grid and the structural model consisting of a beam model and additional control points to facilitate the fluid-structure interaction process

The computational mesh for Navier-Stokes flow analysis is created applying a layer of thin boundary-layer blocks on each aircraft component, i.e. the flow analysis is fully viscous, also on the fuselage, winglets and on the pylons and engine nacelles. Thus, the occurrence of flow separation can be identified everywhere on the aircraft surface. The multi-block mesh generation is, to a large extent, an automatic process. The surface of a configuration is subdivided into a set of faces according to a certain abstraction. Blocks are automatically generated around the abstraction and subsequently mapped into the physical space. Initial settings of the mesh control parameters are also automatically derived. This is possible because of the Cartesian structure of the block topology.

3.2 Structural model

The common way to prepare elasto-mechanical data for the purpose of static aeroelastic analysis with ENFLOW is either by extracting the stiffness matrix and mass matrix from a finite element (FEM) model or by constructing a flexibility matrix from a sequence of static analyses with unit loads at the desired locations. ENFLOW uses 3 degrees of freedom in translation for the communication between the flow solver and the structural solver. For the exercises presented in this paper the elasto-mechanical data have been prepared by AIRBUS-France in the form of a flexibility matrix for the wing which is represented as a beam. At each node of the beam 6 degrees of freedom in translations and rotations are defined. The engines and pylons are



assumed to be rigidly attached to a certain wing station. In order to be able to use these data, several control points are added to the flexibility matrix to comply with the requirements of ENFLOW. The added points are a series of points in each station aligned with the flow direction (to enable the transfer of moment and rotation) and points at the engines and pylons which are connected to the proper attachment points at the wing. Rigid bar relations are used to connect the added control points to the beam. The final control points are illustrated in Figure 4 along with the aerodynamic surface.

The other required elasto-mechanical data are the inertia data concerning the mass distribution. The common way in ENFLOW is to use the mass matrix along with the proper definition of the acceleration. The deformation of the aircraft is then:

$$\vec{x}_{deformed} = \vec{x}_{jig} + [a][\vec{F}_{aerodynamic} + \vec{F}_{inertia} + \vec{F}_{thrust}],$$

where [a] is the flexibility matrix and the inertia force is computed from the mass matrix and acceleration. For the current application, however, the available data concerning the effect of inertia and thrust for a certain flight condition are prescribed in the form of a deformation. Thus, the total deformation is computed as

$$\vec{x}_{deformed} = \vec{x}_{ground} + [a]\vec{F}_{aerodynamic},$$

where the ground shape due to inertia and thrust is defined as

$$x_{ground} = \vec{x}_{jig} + [a][\vec{F}_{inertia} + \vec{F}_{thrust}]$$

3.3 Coupling aerodynamic and structural models

As mentioned previously, the coupling of the aerodynamic and the structural model concerns the synchronisation in space and time. The current synchronisation in time in ENSOLV can be used directly while a slight modification has been applied for the space synchronisation as explained below.

The common way of generating interpolation matrices to connect the aerodynamic and structural surface grids is by using methods based on radial basis functions [3]. This method has many advantages including minimal requirements of user interference, smooth results, exact at the support point and conserving the total force and moment. However, this global method has also disadvantages that showed up during the exercise conducted for the present paper. When the interpolation process is applied in a global manner, the conservation property for the total force and moments will also hold in a global sense. Locally, the conservation property may be violated. It turns out that the total forces and moment for some parts of the structure can be quite different between those computed in the aerodynamic grid and those in the structural grid. These differences seem to be very sensitive to the selection of support points. This problem becomes apparent when applied for the winglet because it resides at the most flexible part of the



wing. The solution to this problem is to generate the interpolation separately for the component. One then has to ensure that the junction between the winglet and the wing is continuous. This is achieved by adding more control points exactly at the line connecting the wing and the winglet.

During fluid structure iterations, the initial aerodynamic grid is adapted to the deformation defined at the surface. The common way in ENFLOW is to define the initial aerodynamic grid to conform with the structural state, i.e. the jig grid or the ground grid. As typical for wings of large aircraft, a relatively large deformation is expected to occur at the desired flight condition. To ease the work of deforming the aerodynamic grid, the initial aerodynamic grid is chosen sufficiently close to the final solution. In the present work, a deformed state of the wing (with standard winglet) at a relevant condition has been used as the initial state for the aerodynamic grid. This state is called the predefined flight shape or in short the flight shape. Thus, only part of the deformation computed in the structural part is transferred to the aerodynamic grid:

$$\vec{x}_{aerodynamic} = \vec{x}_{flight} + [a]\vec{F}_{aerodynamic} + d\vec{x}_{augmentation}$$

where the augmentation deformation is defined as

$$d\vec{x}_{augmentation} = \vec{x}_{ground} - \vec{x}_{flight}$$

3.4 Grid deformation

The basic grid deformation method in ENFLOW is based on a hybrid volume-spline and transfinite interpolation technique. The volume spline is used to deform the block boundaries and the transfinite interpolation is used to deform the volumetric grid inside the blocks[4].

Although the method is known to be robust for various applications involving complex geometries, additional grid control is needed for cases involving high Reynolds number flows. The extreme stiffness of the grid normal to the solid walls to accommodate sufficient resolution in the boundary layers is the cause of occasional grid folding. To resolve the problem, the grids inside the blocks are smoothed further after the basic grid deformation, using a spring analogy method with a special treatment in the stiff direction [5].



4 Results

In this section the results of the static aeroelastic simulation are presented. Prior to analysing the selected test cases, some preliminary static aeroelastic simulations are conducted to verify the methods and the computational models. Subsequently, the results of static aeroelastic simulations for a selection of flight conditions from the flight test program are presented, followed by an analysis of the results. Note that all flight conditions presented here are at level flight. In all conditions the fuel distribution in the wing is held constant, which means that the inertia loads and the ground shape of the wing are also constant. The variations in the results may therefore be interpreted as caused by aerodynamic effects only.

Simulations have been carried out for three configurations, i.e. a configuration without wing tip devices, a configuration with standard winglet and a configuration with large winglet. All results, i.e. bending and twist deformation, are presented with respect to the ground shape at the nodes of the original beam model, which is located at about one-third of the chord from the leading edge.

4.1 Preliminary static aeroelastic simulations

As mentioned previously, an important aspect in the design of a winglet is the orientation with respect to the flow, i.e. the cant angle and toe angle. These angles are influenced by the wing deformation. Therefore the static aeroelastic method should be able to predict the deformation accurately. Preliminary static aeroelastic simulations have been carried out at the design cruise condition at Mach 0.82 and altitude 35000 feet to check two issues. First, for the case of the wing without winglet, it is customary to simplify the deformation to be limited only in the z -direction. Such a simplification significantly eases the fluid-structure interpolation and also the grid deformation. Results of the computations with simplified and full flexibility matrices, however, show that a significant elongation of the wing in the spanwise direction occurs in case of using a simplified flexibility matrix which increases the effective aerodynamic force, resulting in an over-prediction of the deformation. Moreover, as can be seen in Figure 5, the predicted cant angle using a simplified flexibility matrix differs significantly from the case with full flexibility matrix. It is therefore concluded that the full flexibility matrix has to be used.

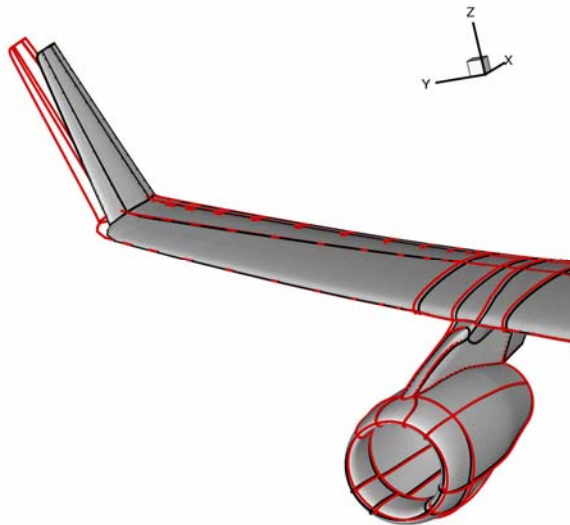


Figure 5 Wing elongation and wrong cant angle as a result of flexibility matrix simplification

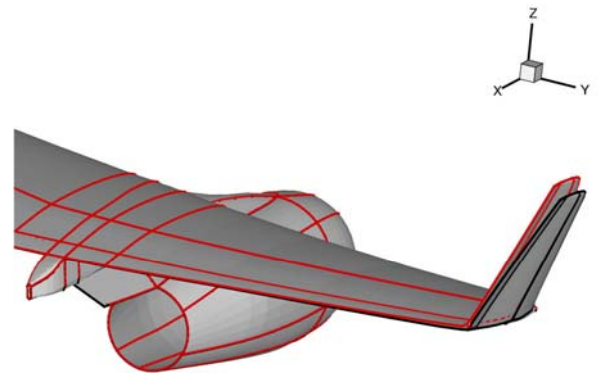


Figure 6 Overview of deformed wing with large winglet computed using global and component-wise interpolation procedure

The second issue concerns the type of interpolation matrix. Two types of interpolation matrices are used: the first one has been generated in a global manner and the second one in a component-wise manner. The first method is the preferred one because it is much easier to carry out. For the component-wise interpolation matrix one has to generate the matrix separately for each component while taking care of the continuity between components. The results of the simulations for the standard winglet do not show significant differences between these two types of interpolation methods. However, for the case of the large winglet, see Figure 6, a significant difference is observed. Quantification of the forces and moments at the winglet, defined on the aerodynamic grid and on the structural grid, reveals differences of up to 30% for the simulations using the global interpolation matrix. This case suggests that the component-wise approach should always be used for non-planar configurations and especially with clearly different scale. As a result of these findings, in the following simulations the full flexibility matrix and the component-wise interpolation matrix are used.

4.2 Comparison with flight test

A selection from the flight test results has been chosen to be used as validation cases for the present static-aeroelastic simulation method. The selected flight conditions are given in Table 1, consisting of three lift coefficients. Some preliminary computations were carried out to obtain an overview of systematic differences between the computed and measured pressure distributions. A satisfactory agreement can be achieved by applying a correction to the free-stream Mach number of 0.005 in the flow calculations, as compared to the flight Mach number. This correction is used for all further comparisons. In the following paragraphs comparisons of



the computed results with the flight test data are discussed for the clean configuration, configuration with standard winglet and configuration with large winglet.

CFD					Flight test				
C_L	Mach	Re	h(feet)	AOA(deg)	C_z	Mach	Re	h(feet)	AOA(deg)
clean configuration									
0.45	0.824	44.7e6	36119	2.16					
0.50	0.824	44.7e6	36119	2.57	0.4938	0.819	44.7e6	36119	2.14
0.60	0.825	42.8e6	36208	3.40	0.5870	0.820	42.8e6	36208	2.69
standard winglet configuration									
0.45	0.825	45.9e6	35715	2.20	0.4430	0.820	45.9e6	35715	1.75
0.50	0.824	45.9e6	36019	2.60	0.4950	0.819	45.9e6	36019	2.13
0.60	0.825	45.6e6	36205	3.43	0.5910	0.820	45.6e6	36205	2.72
large winglet configuration									
0.45	0.825	45.9e6	35715	2.20					
0.50	0.825	45.4e6	35914	2.60	0.4940	0.820	45.4e6	35914	2.11
0.60	0.825	45.6e6	36205	3.43					

Table 1 Selected flight conditions to be used for validation

The comparison of the predicted and measured wing deformations for the clean configuration at the design cruise condition of $C_L=0.50$ is shown in Figure 7 and Figure 8. In addition, a comparison is made for a light weight case $C_L=0.45$ and a heavy weight case $C_L=0.60$. In general, the agreement between the predicted and flight data is very good. The most significant discrepancy is found for the bending deformation at the flight condition with $C_L=0.50$. This discrepancy might be attributed to the inaccuracy in the definition of the ground shape where the contribution of the inertia and engine thrust are taken into account. Considering that the fuel distribution at the wing is maintained constant during the flight test, the only differences should originate from the engine thrust. The thrust force acts in the forward direction parallel to the wing plane, it should therefore contribute negligibly to the upward bending of the wing. However, it exerts a moment onto the wing that reduces the nose-down twist deformations. The level of experimental bending deformation at $C_L=0.50$ can be shown to be matched by computation with C_L of about 0.55. In this case the wing will be twisted slightly too much in nose-down direction compared to the flight test which is in agreement with the previously mentioned conjecture about the effect of engine thrust.

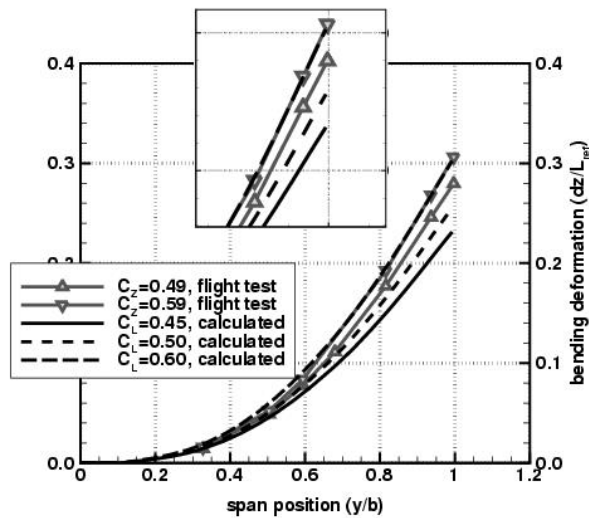


Figure 7 Comparison of predicted and measured wing bending for clean configuration at various C_L values

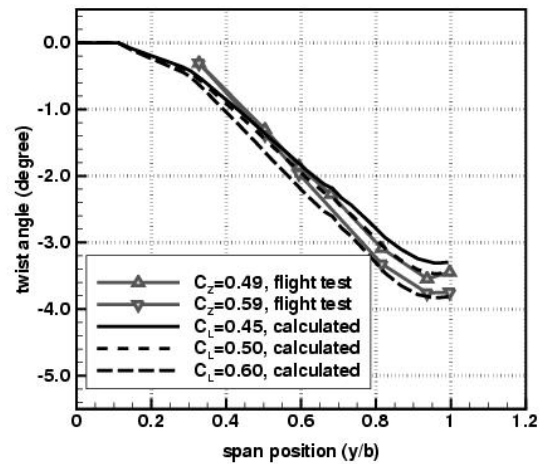


Figure 8 Comparison of predicted and measured wing twist for clean configuration at various C_L values

Next, the results for the configuration with the standard winglet are presented. Comparisons of the predicted wing bending and wing twist with the available flight test data are depicted in Figure 9 and Figure 10 for the lift coefficients of $C_L=0.45, 0.50, 0.60$. The figures show that the overall agreement is good and indicate that the effect of the additional winglet forces on the deformation of the wing is correctly predicted. The observed remaining discrepancies are consistent with the observation made for the clean wing configuration.

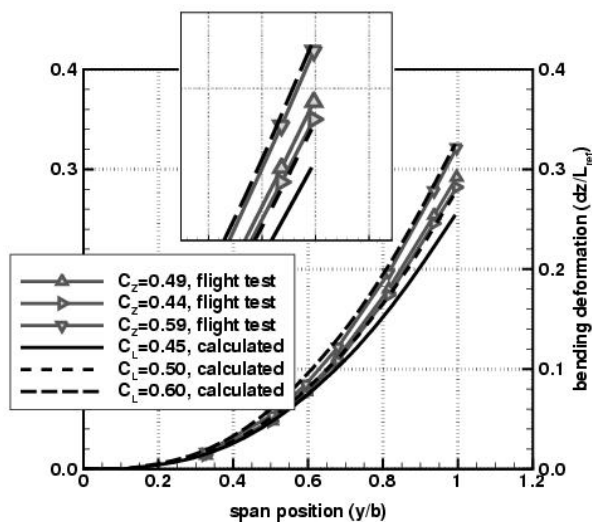


Figure 9 Comparison of predicted and measured wing bending for configuration with standard winglet at various C_L values

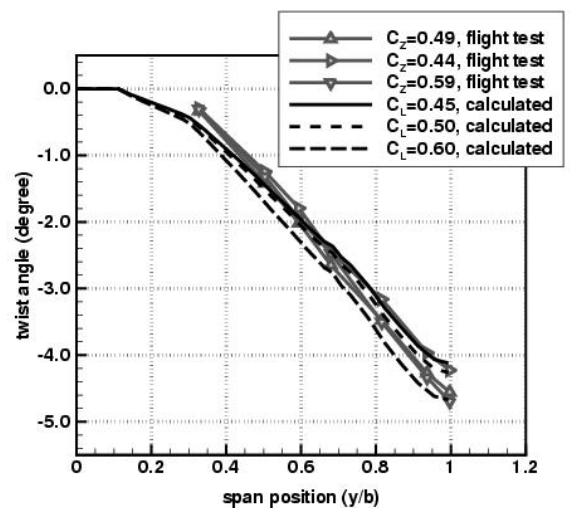


Figure 10 Comparison of predicted and measured wing twist for configuration with standard winglet at various C_L values



The available test data for the large winglet configuration are limited as the flight envelope was only partially cleared for testing (excluding the heavy weight cases). The results of simulations for the configuration with large winglet are compared to the available test data in Figure 11 and Figure 12. Excellent agreement is obtained for the twist-deformation for the lift coefficient of $C_L=0.50$. The bending deformation is, consistent with the other configurations, slightly lower than the measured data from flight test. For the wing equipped with the large winglet, an increment in lift coefficient of $C_L=0.05$ results in a twist-deformation of 0.23 degree and an upward bending of $0.0254 L_{ref}$.

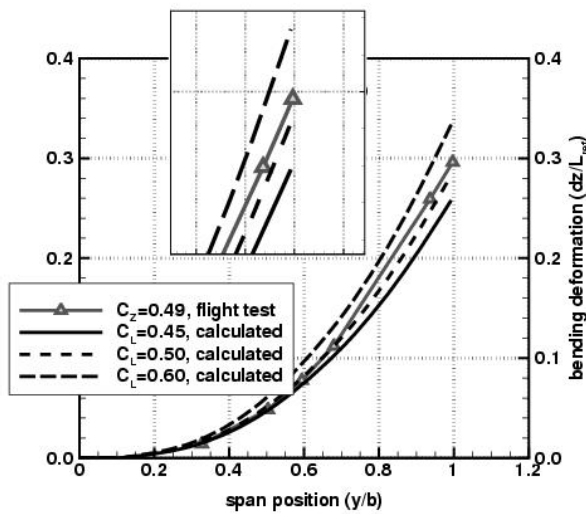


Figure 11 Comparison of predicted and measured wing bending for configuration with large winglet at various C_L values

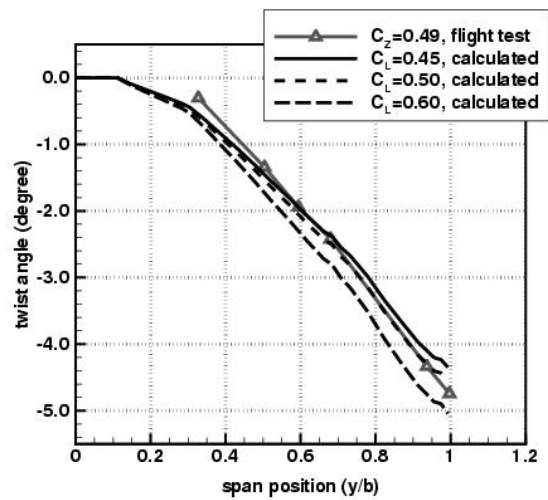


Figure 12 Comparison of predicted and measured wing twist for configuration with large winglet at various C_L values

From the presented comparisons, it may be concluded that good agreements have been obtained between the numerical simulations and the flight data. This gives confidence in the accuracy of method and the correctness of the models used in the present exercise.

4.3 Comparisons between configurations

In this section comparisons of the results are given for various configurations studied in the present project to identify the trends associated with the installation of a winglet to a basic wing. First, from the preliminary computations, comparisons have been made concerning the increase of root bending moment due to the installation of the wing-tip devices. Computations for the flight shape without interaction with the structure for the lift coefficient of $C_L=0.50$

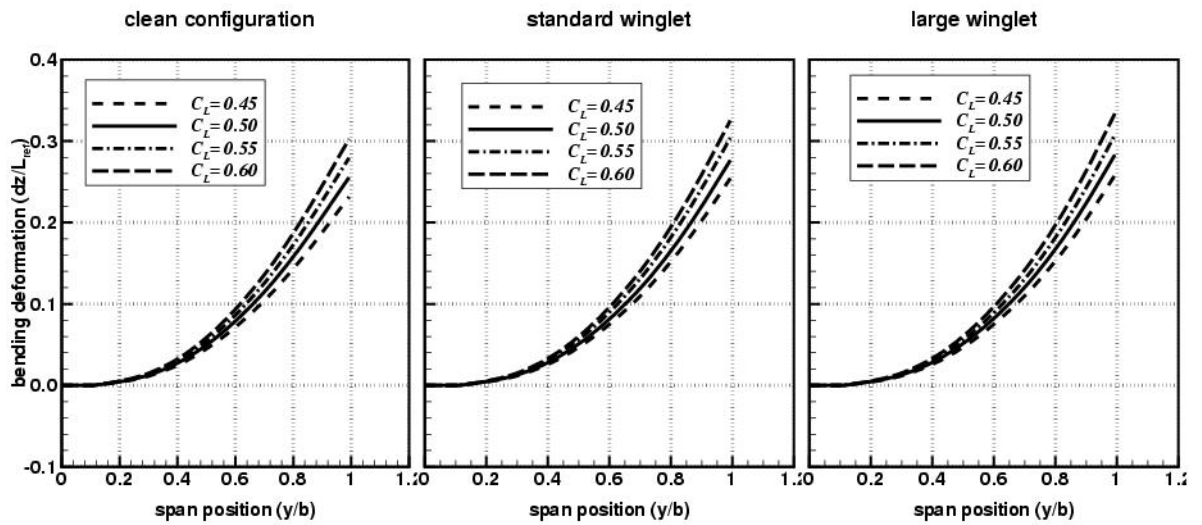


Figure 13 Comparison of predicted wing bending at various C_L values for three wing configurations

reveal that the installation of the standard winglet leads to an increase of 2.6% in wing root bending moment. For the installation of the large winglet an increase of 3.5% is predicted. Taking the flexibility of the structure into account results in a somewhat lower increase of root bending moment of 1.4% for the standard winglet and 1.5% for the large winglet, respectively.

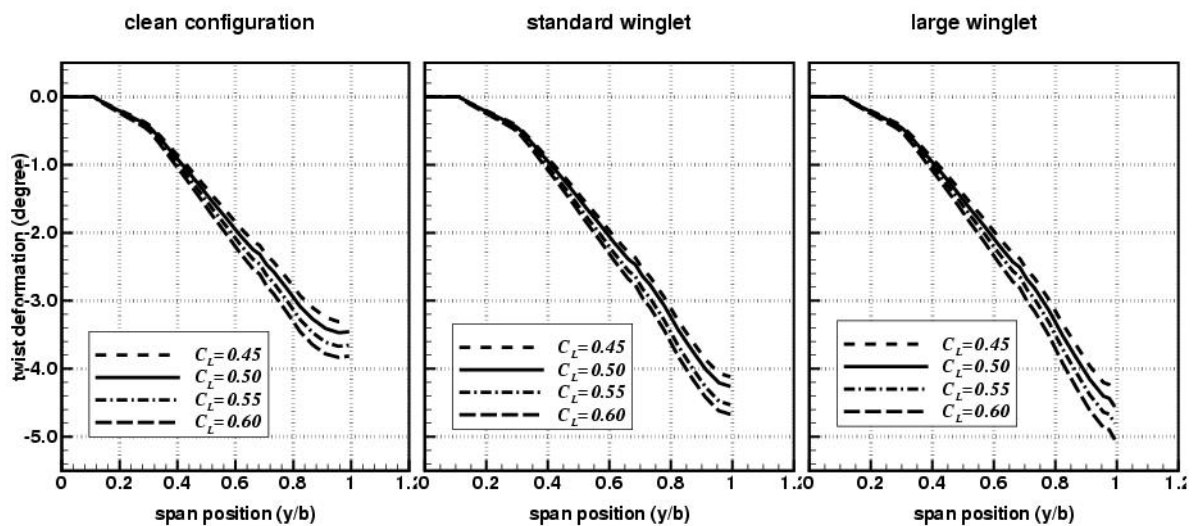


Figure 14 Comparison of predicted wing twist at various C_L values for three wing configurations

The effect of the winglet loads on the wing bending deformations can be deduced from Figure 13. Three families of curves are plotted representing the clean wing tip, standard winglet and large winglet configuration. The members of a family correspond to a specific lift coefficient representative during the cruise phase of the flight. At the design cruise condition, the standard and large winglet lead to an increase in upward wing bending-deformation of $0.0206 L_{ref}$ and $0.0275 L_{ref}$, respectively. The effect of the winglet loads on the wing twist deformations is



plotted in Figure 14. Installation of the standard winglet results in an additional nose-down twist deformation of 0.79 degree at the design lift coefficient of $C_L = 0.50$. Introduction of the large winglet gives an additional nose-down twist of 1.07 degree. The effect of the winglet loads is progressive as winglets become more effective at higher lift coefficients thereby shifting the loads outboard.

5 Concluding Remarks

The impact of winglets of different size on the deformations of a large flexible aircraft is investigated. The purpose of the investigation is to gain understanding of the aeroelastic behaviour of an integrated flexible wing and winglet combination, and to verify and validate methods for the prediction of wing deformations. Three different configurations are investigated: the standard winglet, a large winglet, and the clean wing for reference. Wing deformations are measured in-flight, using optical methods. In view of the rather moderate differences of twist at the wing tip for variations in altitude and lift coefficient, the accuracy of the prediction method needs to be high.

In general, the trends in predicted deformations are in good comparison with measured data, showing that the aerodynamic loads based on Navier-Stokes flow modelling are accurate and suitable for the purpose. A good agreement with measured deformations is observed at higher lift values. Part of the successful prediction of deformations is linked to the availability of a suitable structural model. In the present study, a detailed structural model forms the basis of the flexibility matrix taken into account. The impact of simplifications in the structural model (one degree versus six degrees of freedom of the structural points) leads to larger predictions of bending deformations and smaller predictions of twist deformations. The need for a structural model having six degrees of freedom is especially apparent for non-planar configurations, i.e. wing with winglets.

The issue of suspected influences (e.g. temperature gradients) on the reference ground shape, which is recorded when the aircraft is standing on the platform, requires some further clarification.

The knowledge and experience gained in predicting wing deformations is of utmost importance for design and performance studies in future projects, e.g. linked to active aeroelastic wings and loads control.



6 References

- [1] B.B. Prananta, J.J. Meijer and J van Muijden, *Static aeroelastic simulation using CFD, comparison with linear method*. Paper presented at International Forum on Aeroelasticity and Structural Dynamics 2003, Amsterdam, 2003 also NLR TP-2003-187, NLR, 2003.
- [2] B.B. Prananta, J.C. Kok, S.P. Spekrijse, M.H.L. Hounjet and J.J. Meijer, *Simulation of limit cycle oscillations of fighter aircraft at moderate angle of attack*. Paper presented at International Forum on Aeroelasticity and Structural Dynamics 2003, Amsterdam, 2003 also NLR TP-2003-526, NLR, 2003.
- [3] M.H.L. Hounjet and J.J.Meijer, *Evaluation of elasto-mechanical and aerodynamic data transfer methods for non-planar configurations in computational aeroelastic analysis*. Paper presented International Forum on Aeroelasticity and Structural Dynamics 1995, Manchester, 1995.
- [4] S.P. Spekrijse, B.B. Prananta and J.C. Kok. *A simple, robust and fast algorithm to compute deformations of multi-block structured grids*. NLR TP-2002-105, NLR, 2002.
- [5] B.B. Prananta, M.H.L. Hounjet and H.W.M. Hoeijmakers. *Computational unsteady aerodynamic for aeroelastic applications*. Paper presented at 21st Congress of ICAS, Melbourne, 1999.